Assessing the role of Ca^{2+} in skeletal muscle fatigue using a multi-scale continuum model.

Mina Karami, Begoña Calvo, Hassan Zohoor,
Keikhosrow Firoozbakhsh, Jorge Grasa

PII: S0022-5193(18)30510-1
DOI: https://doi.org/10.1016/j.jtbi.2018.10.034
Reference: YJTBI 9677

To appear in: *Journal of Theoretical Biology*

Received date: 13 June 2018
Revised date: 9 October 2018
Accepted date: 13 October 2018

Please cite this article as: Mina Karami, Begoña Calvo, Hassan Zohoor, Keikhosrow Firoozbakhsh, Jorge Grasa, Assessing the role of Ca^{2+} in skeletal muscle fatigue using a multi-scale continuum model., *Journal of Theoretical Biology* (2018), doi: https://doi.org/10.1016/j.jtbi.2018.10.034

Highlights

- A new multi-scale chemo-mechanical model is presented in order to analyze the role of Ca^{2+} in muscle fatigue and to predict fatigue behavior.
- The output results of isometric simulations were

  tted with experimental data obtained for rabbit Extensor Digitorum Longus muscle.
- Varying the Ca^{2+} concentration level and its kinetics in the tissue, the model was able to predict the evolution of the active force of an experimental fatigue protocol.

Assessing the role of Ca^{2+} in skeletal muscle fatigue using a multi-scale continuum model.

Mina Karami[a], Begoña Calvo[b], Hassan Zohoor[c,d], Keikhosrow Firoozbakhsh[a], Jorge Grasa[b,1]

[a] *School of Mechanical Engineering*
Sharif University of Technology
Azadi Ave., Tehran, Iran

[b] *Aragón Institute of Engineering Research (I3A)*
CIBER-BBN Centro de Investigación en Red en bioingeniería, Biomateriales y Nanomedicina
Universidad de Zaragoza
Campus Río Ebro, Edificio Agustín de Betancourt
C/María de Luna, s/n 50018 Zaragoza, Spain

[c] *Center of Excellence in Design, Robotics and Automation*
Sharif University of Technology
Azadi Ave., Tehran, Iran

[d] *The Academy of Sciences of IR Iran*
Haqqani HWY, Tehran, Iran

Abstract

The Calcium ion Ca^{2+} plays a critical role as an initiator and preserving agent of the cross-bridge cycle in the force generation of skeletal muscle. A new multi-scale chemo-mechanical model is presented in order to analyze the role of Ca^{2+} in muscle fatigue and to predict fatigue behavior. To this end, a cross-bridge kinematic model was incorporated in a continuum based mechanical model, considering a thermodynamic compatible framework. The contractile velocity and the generated active force were directly related to the force-bearing states that were considered for the cross-bridge cycle. In order to determine the values of the model parameters, the output results of an isometric simulation were initially fitted with experimental data obtained for rabbit *Extensor Digitorum Longus* muscle. Furthermore, a simulated force-velocity curve under concentric contractions was compared with reported experimental results. Finally, by

[1] Corresponding author: Jorge Grasa jgrasa@unizar.es

varying the Ca^{2+} concentration level and its kinetics in the tissue, the model was able to predict the evolution of the active force of an experimental fatigue protocol. The good agreement observed between the simulated results and the experimental outcomes proves the ability of the model to reproduce the fatigue behavior and its applicability for more detailed multidisciplinary investigations related to chemical conditions in muscle performance.

Keywords: Skeletal muscle, Fatigue, Chemo-mechanical model, Calcium

1. Introduction

When skeletal muscles are activated repeatedly with intensity, it is well known that the force output declines. But the force is not the only feature affected by fatigue in this tissue: shortening velocity and relaxation behavior are also affected (Allen et al., 2002; Jones, 2010). Although the central nervous system, motor nerves and the neuromuscular junctions can contribute to this phenomenon, the main mechanisms are located in the muscle itself (Allen et al., 2002). A variety of intracellular processes appear to be responsible for fatigue, and these have been assessed and reported extensively in the literature (Westerblad and Allen, 1991, 1993; Allen and Westerblad, 2001; Allen et al., 2002, 2008). Although all of these experiments provide invaluable insights into these mechanisms, according to Röhrle et al. (2012) computer simulations in conjunction with experimental findings can be a powerful tool for evaluating complex hypotheses and conclusions.

Modeling the behavior of skeletal muscle has typically been focused on subcellular processes of a half-sarcomere or on simplified phenomenological relationships to simulate the whole muscle (Röhrle et al., 2012). Regarding the first type of models, the interaction between actin and myosin filaments was initially simulated using a two state model by Huxley (1957). Although this model predicted good results under the mechanical point of view, it was later suggested that the attachment of the cross-bridge occurred at different stages to fulfill heat release outcomes (Huxley, 1973) and transient dynamic responses

(Huxley and Simmons, 1971). The complexity of these models was also reduced to achieve more accessible formulation to simulate macroscopic muscle dynamics (Zahalak, 1981; Wu et al., 1997). Furthermore, new formulations inspired by contractile processes appeared in order to consider dynamic contractions in a half-sarcomere (Razumova et al., 1999, 2000).

Continuous reduction of intracellular Ca^{2+} together with force deficit due to fatigue condition have been proved by experimental investigations on skeletal muscles (Westerblad and Allen, 1991; Allen and Westerblad, 2001). Moreover, the shortening velocity of the tissue is also affected by fatigue, which means a loss of power production and poor performance. These changes in the force-velocity relationship could be caused by Ca^{2+} deficit (Ruiter et al., 2000; Jones, 2010). Since Ca^{2+} is the initiator agent of active behavior in sarcomere, experimental tests suggest a direct relationship between the decay of Ca^{2+} and the functional effects of fatigue (Allen and Westerblad, 2001; Jones, 2010).

In this paper, a multi-scale continuum model that fulfills thermodynamic and mechanical requirements is presented to simulate skeletal muscle contraction under fatigue conditions. First, the chemical phase involved in activation at the sarcomere level is described and formulated in Section 2. The thermodynamic basis that allows the derivation of constitutive laws is presented in Section 3 and is particularized in Section 4. Finally, the assessment and validation of the model using experimental tests is presented in Section 5. The ability of the model to predict the fatigue response of the tissue is discussed in Section 6 together with the formulation proposed and the numerical results obtained.

2. Cross-bridge kinetics

Cross-bridge cycling is responsible for the movement and force production in skeletal muscle cells. In conditions of relaxation, the tropomyosin-troponin complex on the actin filament blocks the actin binding sites and avoids the formation of the cross-bridge with the myosin head. When the Ca^{2+} concentration increases above a certain level or resting threshold, Ca^{2+} binds to troponin and

tropomyosin exposes the myosin binding sites to cross-bridge formation. Since cross-bridges within a half-sarcomere are all in a parallel configuration (Razumova et al., 1999), the generated force equals the sum of forces generated by attached cross-bridges.

Although various models of chemical kinetics in cross-bridge cycling have been suggested (Huxley, 1957; Razumova et al., 2000; Shorten et al., 2007), it has been accepted that an appropriate model for studying the chemomechanical force generation mechanism should have at least three contrasting states (Wahr and Metzger, 1999). The basis for modeling the subcellular level in this work is the model developed by Razumova et al. (1999), which describes myofilament regulation and cross-bridge cycling as a four-state process (Fig. 1). The R_{off} state corresponds to the blocked position of the myosin binding sites by the tropomyosin-troponin complex. As the Ca^{2+} concentration increases, at the D state the regulatory unit unbinds the myosin sites but the cross-bridge is not yet formed. Attachment occurs in A_1 and A_2 states which represent the pre and post-power stroke, respectively.

Transitions through the different states are governed by seven rates k_{on}, k_{off}, f, f', h, h' and g. k_{on} and k_{off} are the rates responsible for the conversion between the "*on*" and "*off*" states of the regulatory unit proportional to the available Ca^{2+} concentration. The forward power stroke is governed by h and detachment is governed by g. The reverse reactions are designated with primes (f' and h') following the same notation as that given by Razumova et al. (1999).

In spite of different types of muscle fibers depending on their metabolism, the behavior of a sarcomere can be generalized to obtain a global muscle response. Therefore in this model, every state represents a fraction of the cross-bridges or a probability of being in one of the defined states fulfilling the constrain relation:

$$R_{\text{off}}(t) + D(t) + A_1(t) + A_2(t) = 1 \tag{1}$$

Considering this constraint equation and the seven rates, the fraction of chemical states can be obtained through solving three ordinary differential equa-

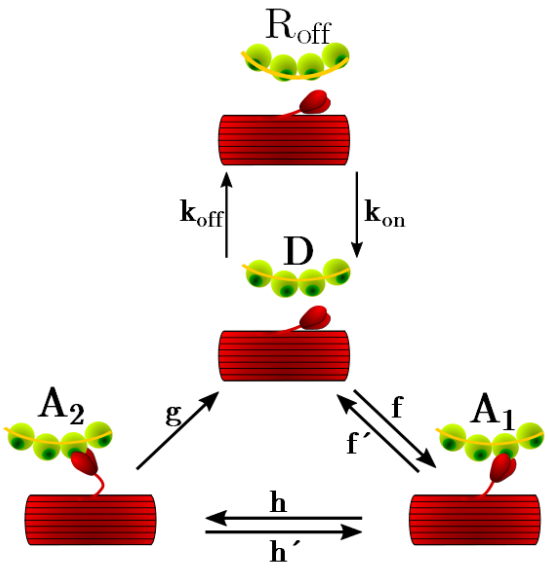

Figure 1: Four-state chemical kinetics (Razumova et al., 1999): R_{off} regulatory unit in "*off*" situation, D regulatory unit in "*on*" but detached situation, A_1 attached pre-power stroke and A_2 attached post-power stroke.

tions:

$$\begin{aligned}
\frac{dD(t)}{dt} &= (f' - k_{\text{on}})\, A_1(t) + (g - k_{\text{on}})\, A_2(t) - (k_{\text{on}} + k_{\text{off}} + f)\, D(t) + k_{\text{on}} \\
\frac{dA_1(t)}{dt} &= f D(t) + h' A_2(t) - (f' + h)\, A_1(t) \qquad (2) \\
\frac{dA_2(t)}{dt} &= h A_1(t) - (h' + g)\, A_2(t)
\end{aligned}$$

The rates which control switching between pre- and post-power stroke states, h and h', and f' have been taken as constants. The rates k_{on} and k_{off} as a function of Ca^{2+} concentration can be expressed as (Campbell et al., 2001):

$$k_{\text{on}} = k_{\text{on}}^0 + \left(k_{\text{on}}^{Ca} - k_{\text{on}}^0\right) \frac{\left[Ca^{2+}\right]^p}{\left[Ca_{50}^{2+}\right]^p + \left[Ca^{2+}\right]^p} \qquad (3)$$

$$k_{\text{off}} = k_{\text{off}}^0 + \left(k_{\text{off}}^{Ca} - k_{\text{off}}^0\right) \frac{\left[Ca^{2+}\right]^p}{\left[Ca_{50}^{2+}\right]^p + \left[Ca^{2+}\right]^p} \qquad (4)$$

in which k_{on}^{Ca} and k_{on}^0 are the rate constants of the regulatory unit with and without activation effect of Ca^{2+}, respectively and k_{off}^{Ca} and k_{off}^0 have an equivalent meaning in the "*off*" situation. $[Ca_{50}^{2+}]$ is the Ca^{2+} concentration level needed for generating 50% of maximum force.

The f rate in Eqs. (2) depends on myofilament distortions and cooperative effects as follows (Razumova et al., 1999):

$$f = f_0 \left[1 + A_1(t) \left(\exp\left(\frac{x_1}{x_0}(v-1)\right) - 1\right) + A_2(t) \left(\exp\left(\frac{x_2}{x_0}(v-1)\right) - 1\right)\right]^2 \qquad (5)$$

where f_0 and v are constant parameters. $v \geq 1$ accounts for the effect of nearest-neighbor cross-bridges in the force-bearing state contribution. The unit value of this parameter represents a zero neighboring effect while a larger number indicates a greater cooperative impact. x_i $(i = 0, 1, 2)$ represents the dimensionless distortion of myofilaments.

The irreversible detached rate is also affected by the distortions as:

$$g = g_0 e^{\varrho(x_2 - x_0)^2} \tag{6}$$

in which g_0 is a constant coefficient and ϱ is a parameter which grades the impact of x_2.

During contraction, elastic deformations or distortions of cross-bridges occur. This average distortion induced by the power stroke during an isometric contraction of a half-sarcomere is denoted by x_0. The average elastic deformations in A_1 and A_2 states induced through filament sliding during non-isometric contractions are denoted by x_1 and x_2, respectively (the reader is referred to the work of Heidlauf and Röhrle (2014) for a graphical interpretation of these deformations). Considering these distortions as dimensionless and averaged for the whole tissue, their evolution can be written modifying those initially proposed by Campbell et al. (2001):

$$\frac{dx_1(t)}{dt} = -\left(f\frac{D(t)}{A_1(t)} + h'\frac{A_2(t)}{A_1(t)}\right)x_1(t) + h'\frac{A_2(t)}{A_1(t)}\left(x_2(t) - x_0\right) + \frac{\dot{\lambda}_a}{2} \tag{7}$$

$$\frac{dx_2(t)}{dt} = -h\frac{A_1(t)}{A_2(t)}\left(x_2(t) - (x_1(t) + x_0)\right) + \frac{\dot{\lambda}_a}{2} \tag{8}$$

where $\dot{\lambda}_a$ is the velocity of the sliding between thick and thin filaments.

3. Thermodynamic model

The deformation associated with muscle activity can be modeled as two fictitious steps (Stålhand et al., 2008; Hernández-Gascón et al., 2013). The first corresponds to the relative motion of the myosin with respect to actin, while the second relates to the elastic deformation of cross-bridges. Mathematically, it can be expressed as a multiplicative decomposition of the tissue stretch as:

$$\lambda = \lambda_a \lambda_e \tag{9}$$

where λ_a defines the deformation associated with the contractile response provoked by the filament sliding, and λ_e represents the deformation due to the cross-bridges elasticity.

3.1. Balance laws

Balance laws for the contracting skeletal muscle are derived by means of the principle of virtual power. This principle states that the external power equals the internal power, denoted by $\mathscr{P}$, plus the change of kinetic energy (Stålhand et al., 2008). By disregarding the temperature, the internal power can be written as the product of so-called forces and first time derivatives of the state variables. In this context, the principle of virtual power can be written as:

$$\mathscr{P} = F\dot{\lambda} + F_a\dot{\lambda}_a + F_{Ca}\dot{\beta} \tag{10}$$

F, F_a and F_{Ca} are the forces related to λ, λ_a and $\beta = [Ca^{2+}]$ the calcium concentration, respectively. Considering the Clausius-Planck inequality and ignoring thermal effects (Holzapfel, 2002):

$$\dot{\Psi} \leq \mathscr{P} \tag{11}$$

where Ψ is the free energy that coincides with the internal energy and is a function of the state and internal variables $\boldsymbol{s} = [R_{\text{off}}, D, A_1, A_2]^T$.

$$\Psi = \Psi(\lambda, \lambda_a, \boldsymbol{s}, \beta) \tag{12}$$

Introducing Eqs. (10) and (12) into Eq. (11):

$$\left(F - \frac{\partial\Psi}{\partial\lambda}\right)\dot{\lambda} + \left(F_a - \frac{\partial\Psi}{\partial\lambda_a}\right)\dot{\lambda}_a - \sum_{i=1}^{4}\frac{\partial\Psi}{\partial s_i}\dot{s}_i + \left(F_{Ca} - \frac{\partial\Psi}{\partial\beta}\right)\dot{\beta} \geq 0 \tag{13}$$

To observe the thermodynamic compatibility, all evolutions of admissible state and internal variables should satisfy the above inequality. The simplest

and most common choice for constitutive equations which satisfy Eq. (13) is to consider the non-dissipative relation for first and third terms:

$$F = \frac{\partial \Psi}{\partial \lambda}, \qquad F_{Ca} = \frac{\partial \Psi}{\partial \beta}. \tag{14}$$

The second term in Eq. (13) is forced to be non-negative as:

$$F_a - \frac{\partial \Psi}{\partial \lambda_a} = C\dot{\lambda}_a \tag{15}$$

where $C \geq 0$ is an arbitrary function. Following Stålhand et al. (2008), a thermodynamic force associated with the chemical states can be defined as:

$$S_i = -\frac{\partial \Psi}{\partial s_i} + a \tag{16}$$

with a as an arbitrary multiplier (Stålhand et al., 2008). Taking the constraint $\sum_{i=1}^{4} s_i = 1$ into account that is equivalent to $\sum_{i=1}^{4} \dot{s}_i = 0$:

$$-\sum_{i=1}^{4} \frac{\partial \Psi}{\partial s_i}\dot{s}_i = \sum_{i=1}^{4} S_i \dot{s}_i \tag{17}$$

On the other hand, it is possible to introduce a linear relation for the thermodynamic force S_i:

$$\sum_{j=1}^{4} x_{ij}\dot{s}_j = S_i \tag{18}$$

Considering Eq. (17) and Eq. (18), inequality (13) will be satisfied for the third term if proposed matrix $\boldsymbol{X}$ with components x_{ij} satisfies the subsequent condition:

$$\dot{\boldsymbol{s}} \cdot \boldsymbol{X}\dot{\boldsymbol{s}} \geq 0 \tag{19}$$

and the related constitutive equation can be derived combining Eqs. (18) and (17):

$$\sum_{j=1}^{4} x_{ij}\dot{s}_j = -\frac{\partial \Psi}{\partial s_i} + a \tag{20}$$

Finally, by suggesting appropriate functions for F_a, F_{Ca} and matrix $\boldsymbol{X}$ in terms of the state variables, it is possible to find β from Eq. (14).b, λ_a from Eq. (15) and the internal variables, s_i, from Eq. (20). Using Eq. (14).a the force F could be obtained for a given stretch λ.

4. Model specialization

As mentioned in the previous section, different functions have to be proposed to obtain the response of the tissue under different levels of activation induced by the calcium concentration. First, the following form of the strain energy is considered:

$$\Psi = \Psi_e(\lambda) + \mathcal{N}(\lambda_a)\Psi_a(\lambda_e, s_i) + \Psi_{\text{XB}}(s_i) + \Psi_c(\beta) \tag{21}$$

where the total energy has been decomposed into several terms related to the energy associated with the passive behavior of the muscle $\Psi_e(\lambda)$, the elastic energy in the cross-bridge attachment $\Psi_a(\lambda_e, s_i)$, the energy in the chemical phase $\Psi_{\text{XB}}(s_i)$ and the energy associated with the calcium concentration $\Psi_c(\beta)$.

A specific 1D form of the free energy in Grasa et al. (2016) is selected for the passive muscle behavior:

$$\Psi_e = c_1(\lambda^2 + \frac{2}{\lambda} - 3) + \Psi'_e \tag{22}$$

$$\Psi'_e = \begin{cases} 0 & \lambda < \overline{\lambda} \\ \dfrac{c_3}{c_4}\left(\exp\left[c_4(\lambda^2 - \overline{\lambda})\right] - c_4(\lambda^2 - \overline{\lambda}) - 1\right) & \lambda > \bar{\lambda} \end{cases}$$

where, c_1, c_3 and c_4 are material constants and $\overline{\lambda}$ defines the transition from the linear to the exponential behavior common in collagen fiber reinforced materials. The energy in the cross-bridge attachment is scaled in Eq. (21) by the overlapping function $0 \leq \mathcal{N}(\lambda_a) \leq 1$ defined as:

$$\mathcal{N} = \exp\left[\frac{-(\lambda_a^{opt} - \lambda_a)^2}{2\xi^2}\right] \tag{23}$$

here λ_a^{opt} represents the stretch of the tissue where the overlapping between the actin and myosin filaments is optimum, that is, muscle develops the maximum force. The parameter ξ governs the band-width of the function. The elastic energy in cross-bridge attachment Ψ_a can be defined as:

$$\Psi_a = (E_1 s_3 + E_2 s_4)\frac{1}{2}(\lambda_e - 1)^2 \tag{24}$$

where E_1 and E_2 are material constants and $(E_1 s_3 + E_2 s_4)$ acts as stiffness of the cross-bridges.

Specific forms of F_a and C functions in Eq. (15) are suggested as follows:

$$F_a = -\nu s_4 \left(\frac{s_3}{\max(s_3)}\right)\mathcal{N}(\lambda_a) \tag{25}$$

$$C = \frac{1}{\mu}(f_1 s_3 + f_2 s_4)\mathcal{N}(\lambda_a) \tag{26}$$

where ν, μ, f_1 and f_2 are constants of the model. F_a can be interpreted as the mechanical force which is generated by the transition of chemical energy during the power stroke. Alternatively, F_a can be considered as the equivalent mechanical friction force between filaments (Gestrelius and Borgström, 1986; Stålhand et al., 2008). In both ways, more cross-bridge connections develop greater forces, hence $s_3/\max(s_3)$ is considered to scale the active force according to the number of connections.

Substituting Eqs. (21-26) into Eq. (15), the evolution law for $\dot{\lambda}_a$ is obtained:

$$\dot{\lambda}_a = \frac{\mu}{(f_1 s_3 + f_2 s_4)} \left[-\nu s_4 \left(\frac{s_3}{\max(s_3)}\right) + (E_1 s_3 + E_2 s_4)\left(\frac{\lambda_e}{\lambda_a}(\lambda_e - 1) - \frac{(\lambda_a - \lambda_a^{opt})}{2\xi^2}(\lambda_e - 1)^2\right)\right] \tag{27}$$

The explicit statement of total stress in skeletal muscle is achieved by introducing Eqs. (21) and (9) in Eq. (14).a as follow:

$$F = \frac{\partial \Psi_e}{\partial \lambda} + \frac{\mathcal{N}(\lambda_a)}{\lambda_a}\frac{\partial \Psi_a}{\partial \lambda_e} \tag{28}$$

Regarding the chemical phase, the third term in Eq. (21), $\Psi_{\mathrm{XB}}(s_i)$ is associated with cross-bridge free energy and can be additively decomposed assuming no coupling between the states (Stålhand et al., 2008). To find the chemical states s_i, in addition to assigning the $\Psi_{\mathrm{XB}}(s_i)$ function, it would be necessary to find matrix $\boldsymbol{X}$ which can be a function of λ_a, λ_c and β. Therefore, specifically designed experiments would be required to find the coefficients for $\Psi_{\mathrm{XB}}(s_i)$ and components of $\boldsymbol{X}$. To the best of the authors' knowledge, no such investigation which measures the chemical and mechanical coupling in sarcomeres has been reported in the literature. However, Stålhand et al. (2008) proved that a system of differential equations like Eq. (2) is a specific form of Eq. (20). Therefore, in this study s_i have been obtained solving Eq. (2).

The last term of Eq. (21), $\Psi_C(\beta)$ is the free energy related to the calcium ion concentration in the skeletal muscle cell. Considering Eq. (14).b, the simplest function for this chemical free energy (Stålhand et al., 2008) is:

$$\Psi_C = \frac{1}{2}\beta^2 \tag{29}$$

The chemical force, F_{Ca}, can be evaluated for a non-dissipative chemical state by introducing Eqs. (29) and (21) in (14) giving the result:

$$F_{Ca} = \beta \tag{30}$$

With the information about Ca^{2+}, assigning initial values to the four cross-bridge states, the two myofilament distortions and assuming that at the beginning of force generating $\dot{\lambda}_a = 0$, it would be possible to solve Eqs (2), (7), (8) and (1). The initial values of $[R_{\mathrm{off}}, D, A_1, A_2, x_1, x_2]$ have been chosen as $[0.999997, 10^{-5}, 10^{-5}, 10^{-5}, 0, 10^{-2}/1.6]$, respectively. With these levels, the active velocity of contraction $\dot{\lambda}_a$ can be updated using Eq. (27). Therefore, active

and elastic stretches can be computed using $\dot{\lambda}_a$ along with Eq. (9). Finally, the muscle force will be determined using Eq. (28). The solving process can be summarized with the equation system as follows:

$$\begin{aligned} \textstyle\sum_{i=1}^{4} s_i &= 1 \\ [\dot{s}_i] &= A_{ij}\left(Ca, \boldsymbol{x}\right) s_j + B_i \quad i = 2-4 \\ [\dot{x}_i] &= C_{ij}\left(Ca, \boldsymbol{s}\right) x_j + D_i \quad i = 1-2 \\ \dot{\lambda} &= E\left(\boldsymbol{x}, \boldsymbol{s}, \lambda_a, \lambda_e\right) \\ F &= F\left(\boldsymbol{s}, \lambda_a, \lambda_e\right) \end{aligned} \tag{31}$$

5. Model assessment and results

To study the ability of the model to predict muscle fatigue, different assumptions for the parameters that define its behavior were established due to the lack of experimental results for identical animal species. Initially, as shown in the following section, the unfatigued behavior of the muscle was analyzed to reproduce a single tetanic contraction and the force-velocity relationship. Then, the effect of the Ca^{2+} concentration was assessed in the force/stress response. Finally, the model was adjusted to reproduce the results reported by Sierra et al. (2017) for the rabbit *Extensor Digitorum Longus* (EDL) muscle, which provided the muscle force evolution during repeated isometric contractions.

5.1. Model configuration and validation

As mentioned, Ca^{2+} release from the sarcoplasmic reticulum is the input of the model which starts the cross-bridge cycling and the production of muscle force. In this work, the Ca^{2+} evolution has been taken from experimental data reported in the literature (Calderón, 2013) avoiding the definition of a mathematical expression for β and consequently for Ψ_C and F_{Ca}. However, in (Calderón, 2013) the maximum level of the steady-state calcium concentration for the EDL muscle was not reported. Therefore, a single Ca^{2+} transient signal has been scaled following data reported in Stephenson and Williams (1982).

Furthermore, other calcium properties ($[Ca_{50}^{2+}]$ and p in Eqs. (3) and (4)) have been obtained from the F-pCa curve of the EDL muscle reported in Stephenson and Williams (1982) ($pCa = -log([Ca^{2+}])$ and $pCa_{50} = -log([Ca_{50}^{2+}])$, see Table 1). The calcium signal for maximal (tetanic) or submaximal contractions was obtained by the summation of the twitch signal according to the stimulation time and frequency.

A Matlab nonlinear least-squares curve fitting program was used to adjust the simulation result with the experimental isometric contraction of rabbit EDL muscle (Sierra et al., 2017). This fitting allowed all the parameters involved in the model to be obtained using as initial seeds those proposed by Razumova et al. (1999) for the rates related to cross-bridge dynamics. The passive mechanical behavior was taken from the literature (Calvo et al., 2010). A summary of the final parameter values is presented in Table 1 distinguishing between those related to cross-bridges, macroscopic mechanical behavior and calcium kinetics. The simulated isometric stress for a 0.2 s contraction stimulated at 100 Hz together with the experimental contraction of the unfatigued EDL muscle is represented in Fig. 2. The isometric stress reaches the maximum value (0.433 MPa) at 0.14 s, remains at this level for a short time and starts to decrease with slow and then fast rates.

The ability of the model to reproduce concentric contractions was also evaluated. A set of different load levels was introduced to obtain the well-known force-velocity relationship. In Fig. 3 the simulation results are compared to the experimental data of EDL rat muscle at $35°C$ (Ranatunga, 1984)). The muscle response is presented as the shortening velocity against different percentages of the maximum isometric stress. With increasing the resistance tension stress from 5% to 50% of maximum isometric stress, the shortening velocity was decreased from 125.2 to 29.9 mm/s.

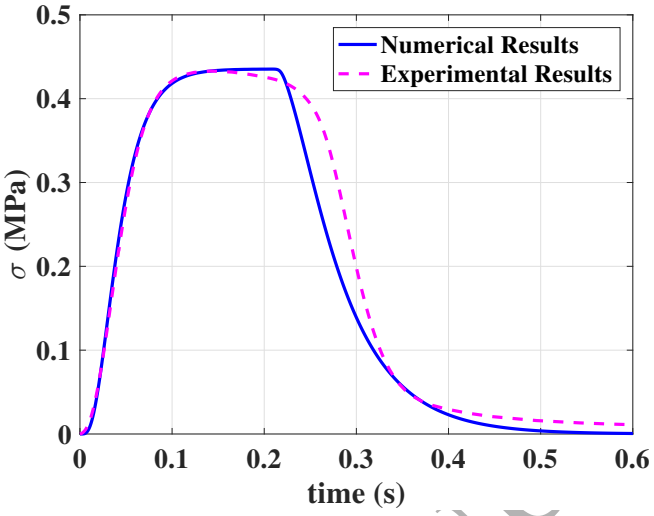

Figure 2: Isometric contraction for unfatigued EDL muscle of rabbit (the dashed line shows the experimental data (Sierra et al., 2017) and the solid line the model simulated result)

Cross Bridge Parameters

k^0_{on} (1/s)	0	f_0 (1/s)	123.623	g_0 (1/s)	1.001
k^{Ca}_{on} (1/s)	51.937	f' (1/s)	477.470	ϱ (-)	1
k^0_{off} (1/s)	12.115	h (1/s)	8.213	v (-)	1.001
k^{Ca}_{off}. (1/s)	174.778	h' (1/s)	50.626	x_0 (-)	0.006

Mechanical Parameters

E_1 (N)	143.815	ν (N)	51	c_1 (N)	0.001
E_2 (N)	567.842	μ (-)	2.229	c_3 (N)	0.054
f_1 (N·s)	9.113	ξ (-)	0.164	c_4 (N)	0.783
f_2 (N·s)	13.058	λ_{opt} (-)	1	$\overline{\lambda}$ (-)	1.254

Calcium Properties

pCa_{max}	4.975	pCa_{50}	5.816	p	4

Table 1: Model parameters determined for the EDL rabbit muscle. The parameters were obtained fitting the passive and active behavior characterized experimentally.

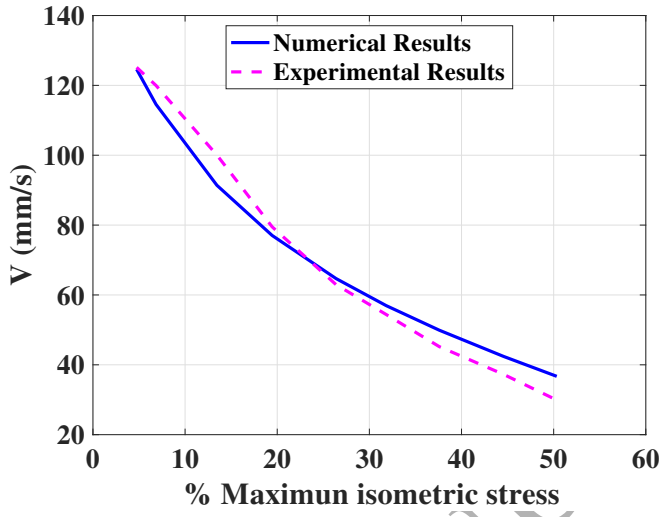

Figure 3: Experimental (Ranatunga, 1984) and simulated force-velocity relationship for rat EDL muscle.

5.2. Fatigue simulation

Once the potential of the model has been assessed for isometric and concentric contractions, in this section the role of calcium is evaluated during fatigue. As mentioned, this phenomenon has a distinctive effect on the mechanical performance of muscles and is associated with a depression in both the $[Ca^{2+}]$ level and the myofibrillar sensitivity. However, the $[Ca^{2+}]$ binding cooperatively remains the same (Chin and Allen, 1998; Debold et al., 2006; Fitts, 2008). In fact, an increase in the level of $[Ca_{50}^{2+}]$, requires more $[Ca^{2+}]$ to produce the same level of force. Experimental results of the $[Ca_{50}^{2+}]$ increment in fast skeletal muscle fiber reported by Chin and Allen (1998) have been extrapolated according to the intensity of the fatigue test (stimulating the muscle with 100 Hz every 10 second for one hour (Sierra et al., 2017)). It has also been assumed that $[Ca_{50}^{2+}]$ will change linearly at different levels of fatigue as well.

Fig. 4 represents the experimental evolution of maximal repetitive isometric contractions of rabbit EDL muscle (Sierra et al., 2017). The tissue was stimulated under tetanic conditions for 0.2 s every 10 s during one hour. As

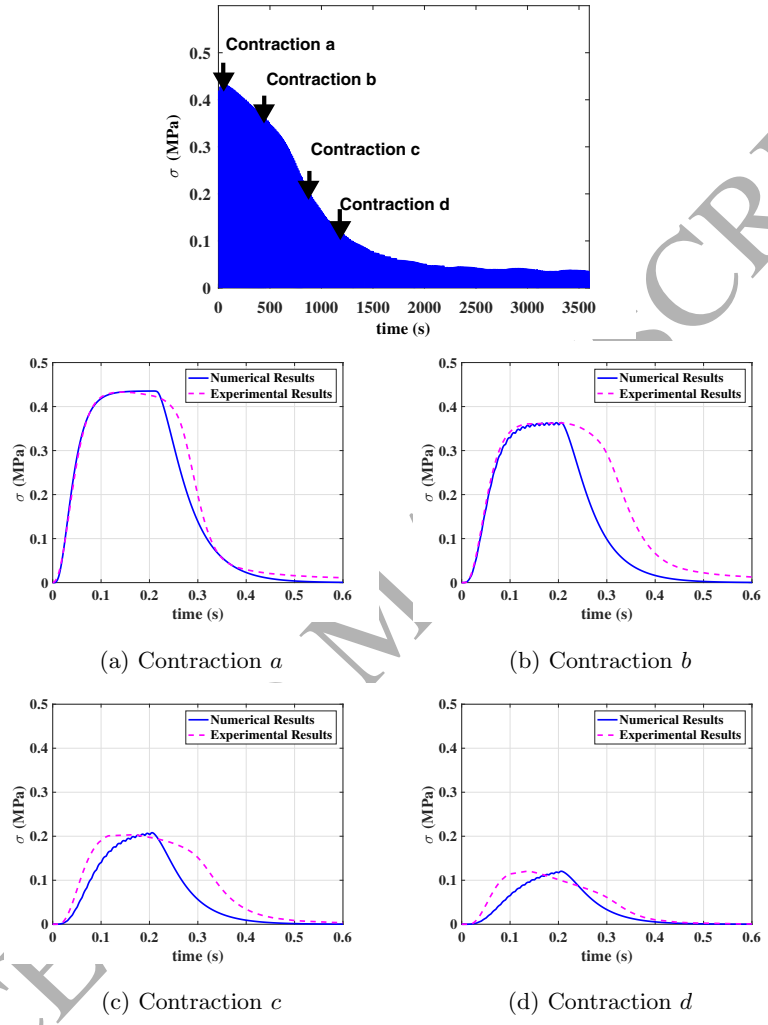

(a) Contraction a (b) Contraction b

(c) Contraction c (d) Contraction d

Figure 4: Four experimental and the equivalent simulated isometric contractions of rabbit EDL muscle fatigue tests. (Top panel) Continuous tetanic contraction; each vertical line shows a tetanus which is simulated for 0.2 s with 100 Hz after 10 s rest. (Bottom panel) Four extracted contraction-relaxation cycles of rabbit EDL in (a) unfatigued muscle, (b) 16%, (c) 53% and (d) 72% reduction of maximum force due to fatigued conditions.

	pCa	pCa_{50}
Contraction a	4.9748	5.8158
Contraction b	5.7017	5.8111
Contraction c	5.9111	5.8004
Contraction d	5.9807	5.7949

Table 2: Ca^{2+} concentration levels for the four simulated contractions (at 30 s, 400 s, 800 s and 1200 s) considered in the fatigue processes.

indicated in the figure (vertical arrows) four contractions have been considered to fit with the model. The first contraction (a) was selected at the beginning of the test when the maximum isometric stress is reached. In the second selected contraction, the muscle developed approximately 84% (b), in the third 47% (c) and in the last 28% of its maximum stress. The fitting results for these four contractions can be observed in the same figure with the experimental contractions. Estimated levels of pCa and pCa_{50} for these simulated contractions are presented in Table 2, varying from $pCa = 4.9748$ and $pCa_{50} = 5.8158$ in the unfatigued contraction to $pCa = 5.9807$ and $pCa_{50} = 5.7949$ for the highest fatigue level. As can be observed, $[Ca^{2+}]$ has to decrease to fit the maximum level of force.

Using the $[Ca^{2+}]$ and $[Ca_{50}^{2+}]$ levels determined for the four selected fatigued contractions in Fig. 4, the force-velocity relationship has been reproduced for a set of external loads from 5% to 80% of the maximum generated force in each condition (Fig. 5). In Fig. 5, the predicted velocity has been normalized by the maximum velocity of the unfatigued condition. As can be observed, the results of the model show that along with the increase in the fatigue level, the contractile velocity of the muscle decreases, that is, the most fatigued condition has the lowest shortening velocity. Moreover, the velocity reduction has a non-linear behavior looking at fixed levels of the resistance force reached.

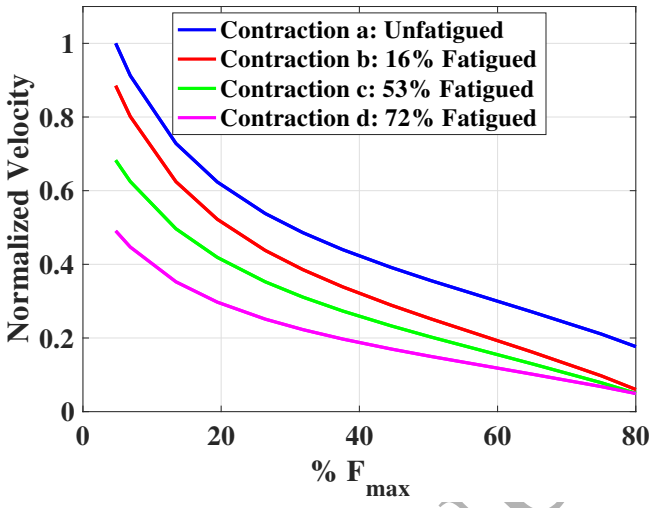

Figure 5: Simulated force-velocity curve in unfatigued and fatigued conditions. *Ca* properties in each condition are reported in Table 2. Velocity data has been normalized to the maximum value of the unfatigued contraction.

6. Discussion

The multi-scale model developed in this work, using the $[Ca^{2+}]$ level as an input governing parameter of the skeletal muscle contraction, is able to reproduce the most important characteristic features of fatigue such as force deficit, reduction in shortening velocity and alterations in the contraction-relaxation cycle. In previous studies related to muscle fatigue, it has been accepted that this force decreasing phenomenon is a consequence of a lower number of connections in post- and pre-power stroke states (Fitts, 2008; Place et al., 2009; Jones, 2010). Although the variation in other chemical factors could influence the characteristics of the Ca^{2+} signal and functional features of the muscle (Allen and Westerblad, 2001; Godt and Nosek, 1989; Debold et al., 2016; Allen et al., 2008), they have not been considered in this model. This limitation could be responsible of the differences in the fitting of the relaxation phase and in the fatigued states in Figs. 2 and 4.

Cross bridge cycling starts after an increase in the Ca^{2+} concentration level,

and the proportion of connections in the force bearing states (A_1 and A_2) are determined according to different transition rates. The available experimental information for these rates is limited to just two states (attached or detached) of the actin and myosin filaments (Brenner, 1988; Metzger et al., 1989; Sweeney and Stull, 1990; Rome et al., 1999). The initial data in the model has been taken from Razumova et al. (1999) which corresponds to a proposed feasible group of rate coefficients and those in Campbell et al. (2001) and Rice et al. (2008) relating to cardiac muscle fibers. The final rates found in the present model by fitting the experimental rabbit EDL results are slightly different from those mentioned and in general very similar to other muscles and species. For example, the detachment rate ($g = 1.0004\ s^{-1}$) is in the range of previously reported experimental measurements for rabbit fast-twitch psoas (Rome et al., 1999).

It has also been shown that these rates depend on various factors such as calcium concentration (Metzger and Moss, 1990), myofilaments distortion, cooperation effects (Razumova et al., 2000) and temperature (Stephenson and Williams, 1981; Rice et al., 2008). Although the dependency on temperature has been neglected, the effects of other parameters have been considered, even if in a simple form. According to Eqs. (3) and (4), the k_{on} and k_{off} rates change their rest value (k_{on}^0 and k_{off}^0) depending on the Ca^{2+} concentration. As the XB kinematics cycle starts according to the k_{on} and k_{off} values, all four states of the XB cycle will be affected by $[Ca^{2+}]$ (Razumova et al., 2000). As mentioned before, the v parameter in Eq. (5) models the effect of the XB neighboring contribution on f rate. Consequently, f_0 in Eq. (5) is equivalent to the f rate when none of the neighboring XBs are in force bearing condition (pre- and post-power stroke - A_1 and A_2) ($v = 1 \Rightarrow f = f_0$). On the other hand, myofilaments distortion will change the space between contiguous XBs and accordingly their level of contribution to the force bearing status. Therefore, in the f rate the nearest neighbor influence has been scaled with respect to the myofilament distortion (x_1, x_2) (Razumova et al., 1999). Moreover, the detachment rate g depends on the myofilament distortion in the post-power stroke condition (x_2). Accord-

ing to Eq. (6), g_0 can be interpreted as the detachment of XBs in isometric condition (Razumova et al., 1999).

The derivation of constitutive equations from balance laws (Stålhand et al., 2008; Hernández-Gascón et al., 2013) has resulted in a good performance in numerical simulations of living tissues (Stålhand et al., 2011; Grasa et al., 2016). The incorporation of cross-bridge cycling at the micro level to the elastic energy function has required some additional approximations. Although Razumova et al. (1999) considered a fixed value of stiffness for the cross-bridges attached states (A_1 and A_2), the model assumed different stiffnesses (E_1 and E_2, respectively). These macroscopic stiffnesses are actually the product of the corresponding state stiffness in the sarcomere level by the total number of related attachments in the whole muscle. The larger value of E_2 compared to E_1 is related to the hypothesis that the post-power stroke attachment is stronger than the pre-power stroke (Jones, 2010; Fitts, 2008). Moreover, there is some experimental evidence that during fatigue condition the stiffness per cross-bridge decreases (Fitts, 2008; Place et al., 2009; Nocella et al., 2017). However, this variation has been ignored.

Data recorded from calcium distribution signals in single fibers of skeletal muscle under fatigue conditions have confirmed that $[Ca^{2+}]$ declines along with the fatigue phenomenon (Westerblad and Allen, 1993, 1991). Moreover, under fatigue conditions, the resting threshold of Ca^{2+} rises as a consequence of a decrease in calcium sensitivity. This circumstance is accompanied by a $[Ca_{50}^{2+}]$ increase. It has been shown that with decreasing $[Ca^{2+}]$ and increasing $[Ca_{50}^{2+}]$, the presented model is able to predict different levels of fatigue. However, experimental studies of fatigue have demonstrated that in addition to the intracellular Ca^{2+} variation, the rate of sarcoplasmic reticulum (SR) Ca^{2+} uptake also varies (Westerblad and Allen, 1993). This SR environment and its chemical kinetics has not been considered in the present model. Furthermore, according to the literature (Westerblad and Allen, 1993; Rome, 2006), one of the effective factor in skeletal muscle relaxation is Ca^{2+} uptake. Differences between the experimental data and simulated results in the relaxation part of the contraction cycle

could be due to neglecting these effects.

The shortening velocity against constant resistive forces in concentric conditions has also been simulated after fatigue (Fig. 5). Similar to experimental findings (Haan et al., 1989; Curtin and Edman, 1994; Ruiter et al., 2000), the model is able to predict the decreasing effect on the velocity of contraction along with the increase in fatigue level.

7. Conclusions

A multi-scale chemo-mechanical model for predicting the active behavior of skeletal muscle under both unfatigued and fatigued conditions has been presented. The constitutive framework of the model adheres to the thermodynamic laws so that it is suitable to be applied in 3D simulations. A comparison of the computational results with experimental data demonstrates the ability of the model to simulate isometric and concentric contractions and the force-velocity relationship in skeletal muscles. Due to the lack of experimental results to determine the whole set of parameters for the same animal species, slightly differences counteracting effects in the proposed values could provide the same model outcome. Thereby, the selection was made carefully always in the range of the parameters available in the literature.

The chemical features of the model make it appropriate for investigating chemically dependent phenomena such as fatigue. Good agreement was found between the simulated and experimental results in the force development of fatigued muscle. Moreover, it has been shown that the model can predict the reduction of contractile velocity as a consequence of fatigue inefficiency. As the model is activated by the calcium ion transient signal, it would be possible to predict different levels of muscle activation (twitch summation) based on the calcium signal accumulation. Therefore, when defining the relation between electrical stimulation and released intracellular calcium ion, the model could be useful for simulating techniques such as Functional Electrical Stimulation.

8. Acknowledgements

The authors gratefully acknowledge research support from the Spanish Ministry of Economy and Competitiveness (Grants DPI2014-54981-R and DPI2017-84047-R) and the Gobierno de Aragón for the support of group T24_17R. The first author is grateful for research support from the Iranian Ministry of Science, Research and Technology.

The authors also acknowledge the support of the Tissue Characterization Platform of CIBER-BBN, an initiative funded by the VI National R&D&i Plan 2008-2011, Iniciativa Ingenio 2010, Consolider Program, CIBER Actions and financed by the Instituto de Salud Carlos III with assistance from the European Regional Development Fund.

9. References

References

Allen D, Westerblad H. Role of phosphate and calcium stores in muscle fatigue. The Journal of physiology 2001;536(3):657–65.

Allen DG, Kabbara AA, Westerblad Hk. Muscle fatigue: the role of intracellular calcium stores. Can J Appl Physiol 2002;27(1):83–96.

Allen DG, Lamb GD, Westerblad H. Skeletal muscle fatigue: cellular mechanisms. Physiological reviews 2008;88(1):287–332.

Brenner B. Effect of ca2+ on cross-bridge turnover kinetics in skinned single rabbit psoas fibers: implications for regulation of muscle contraction. Proceedings of the National Academy of Sciences 1988;85(9):3265–9.

Calderón JC. Enzymatic dissociation of long muscles from mice: a model for the study of skeletal muscle fiber types. Iatreia 2013;26(2):117–26.

Calvo B, Ramírez A, Alonso A, Grasa J, Soteras F, Osta R, Muñoz M. Passive nonlinear elastic behaviour of skeletal muscle: experimental results and model formulation. Journal of biomechanics 2010;43(2):318–25.

Campbell KB, Razumova MV, Kirkpatrick RD, Slinker BK. Nonlinear myofilament regulatory processes affect frequency-dependent muscle fiber stiffness. Biophysical Journal 2001;81(4):2278–96.

Chin E, Allen D. The contribution of ph-dependent mechanisms to fatigue at different intensities in mammalian single muscle fibres. The Journal of physiology 1998;512(3):831–40.

Curtin N, Edman K. Force-velocity relation for frog muscle fibres: effects of moderate fatigue and of intracellular acidification. The Journal of physiology 1994;475(3):483–94.

Debold EP, Fitts RH, Sundberg CW, Nosek TM. Muscle fatigue from the perspective of a single crossbridge. Med Sci Sports Exerc 2016;48(11):2270–80.

Debold EP, Romatowski J, Fitts RH. The depressive effect of pi on the force-pca relationship in skinned single muscle fibers is temperature dependent. American Journal of Physiology - Cell Physiology 2006;290(4):C1041–50. doi:10.1152/ajpcell.00342.2005.

Fitts RH. The cross-bridge cycle and skeletal muscle fatigue. Journal of applied physiology 2008;104(2):551–8.

Gestrelius S, Borgström P. A dynamic model of smooth muscle contraction. Biophysical journal 1986;50(1):157–69.

Godt RE, Nosek TM. Changes of intracellular milieu with fatigue or hypoxia depress contraction of skinned rabbit skeletal and cardiac muscle. The Journal of Physiology 1989;412(1):155–80.

Grasa J, Sierra M, Lauzeral N, Munoz M, Miana-Mena F, Calvo B. Active behavior of abdominal wall muscles: Experimental results and numerical model formulation. Journal of the mechanical behavior of biomedical materials 2016;61:444–54.

Haan A, Jones D, Sargeant A. Changes in velocity of shortening, power output and relaxation rate during fatigue of rat medial gastrocnemius muscle. Pflügers Archiv European Journal of Physiology 1989;413(4):422–8.

Heidlauf T, Röhrle O. A multiscale chemo-electro-mechanical skeletal muscle model to analyze muscle contraction and force generation for different muscle fiber arrangements. Front Physiol 2014;5:498. doi:10.3389/fphys.2014.00498.

Hernández-Gascón B, Grasa J, Calvo B, Rodríguez JF. A 3D electro-mechanical continuum model for simulating skeletal muscle contraction. J Theor Biol 2013;335:108–18. doi:10.1016/j.jtbi.2013.06.029.

Holzapfel GA. Nonlinear solid mechanics: a continuum approach for engineering science. Meccanica 2002;37(4):489–90.

Huxley AF. Muscle structure and theories of contraction. Prog Biophys Biophys Chem 1957;7:255–318.

Huxley AF. A note suggesting that the cross-bridge attachment during muscle contraction may take place in two stages. Proc R Soc Lond B Biol Sci 1973;183(1070):83–6.

Huxley AF, Simmons RM. Proposed mechanism of force generation in striated muscle. Nature 1971;233(5321):533–8.

Jones DA. Changes in the force–velocity relationship of fatigued muscle: implications for power production and possible causes. The Journal of physiology 2010;588(16):2977–86.

Metzger JM, Greaser ML, Moss RL. Variations in cross-bridge attachment rate and tension with phosphorylation of myosin in mammalian skinned skeletal muscle fibers. implications for twitch potentiation in intact muscle. The Journal of general physiology 1989;93(5):855–83.

Metzger JM, Moss RL. Calcium-sensitive cross-bridge transitions in mammalian fast and slow skeletal muscle fibers. Science 1990;247(4946):1088–91.

Nocella M, Cecchi G, Colombini B. Phosphate increase during fatigue affects crossbridge kinetics in intact mouse muscle at physiological temperature. The Journal of Physiology 2017;.

Place N, Bruton JD, Westerblad H. Mechanisms of fatigue induced by isometric contractions in exercising humans and in mouse isolated single muscle fibres. Clinical and Experimental Pharmacology and Physiology 2009;36(3):334–9.

Ranatunga K. The force-velocity relation of rat fast-and slow-twitch muscles examined at different temperatures. The Journal of Physiology 1984;351(1):517–29.

Razumova MV, Bukatina AE, Campbell KB. Stiffness-distortion sarcomere model for muscle simulation. Journal of Applied Physiology 1999;87(5):1861–76.

Razumova MV, Bukatina AE, Campbell KB. Different myofilament nearest-neighbor interactions have distinctive effects on contractile behavior. Biophysical Journal 2000;78(6):3120–37.

Rice JJ, Wang F, Bers DM, De Tombe PP. Approximate model of cooperative activation and crossbridge cycling in cardiac muscle using ordinary differential equations. Biophysical journal 2008;95(5):2368–90.

Röhrle O, Davidson JB, Pullan AJ. A physiologically based, multi-scale model of skeletal muscle structure and function. Front Physiol 2012;3:358. doi:10.3389/fphys.2012.00358.

Rome LC. Design and function of superfast muscles: new insights into the physiology of skeletal muscle. Annu Rev Physiol 2006;68:193–221.

Rome LC, Cook C, Syme DA, Connaughton MA, Ashley-Ross M, Klimov A, Tikunov B, Goldman YE. Trading force for speed: why superfast crossbridge

kinetics leads to superlow forces. Proceedings of the National Academy of Sciences 1999;96(10):5826–31.

Rome LC, Syme DA, Hollingworth S, Lindstedt SL, Baylor SM. The whistle and the rattle: the design of sound producing muscles. Proceedings of the National Academy of Sciences 1996;93(15):8095–100.

Ruiter Cd, Didden W, Jones D, Haan Ad. The force-velocity relationship of human adductor pollicis muscle during stretch and the effects of fatigue. The Journal of physiology 2000;526(3):671–81.

Shorten PR, O'Callaghan P, Davidson JB, Soboleva TK. A mathematical model of fatigue in skeletal muscle force contraction. Journal of muscle research and cell motility 2007;28(6):293–313.

Sierra M, Grasa J, Muñoz M, Miana-Mena F, González D. Predicting muscle fatigue: a response surface approximation based on proper generalized decomposition technique. Biomechanics and modeling in mechanobiology 2017;16(2):625–34.

Stålhand J, Klarbring A, Holzapfel GA. Smooth muscle contraction: mechanochemical formulation for homogeneous finite strains. Progress in biophysics and molecular biology 2008;96(1):465–81.

Stålhand J, Klarbring A, Holzapfel GA. A mechanochemical 3d continuum model for smooth muscle contraction under finite strains. J Theor Biol 2011;268(1):120–30. doi:10.1016/j.jtbi.2010.10.008.

Stephenson D, Williams D. Effects of sarcomere length on the force—pca relation in fast-and slow-twitch skinned muscle fibres from the rat. The Journal of Physiology 1982;333(1):637–53.

Stephenson D, Williams Dt. Calcium-activated force responses in fast-and slow-twitch skinned muscle fibres of the rat at different temperatures. The Journal of Physiology 1981;317(1):281–302.

Sweeney HL, Stull JT. Alteration of cross-bridge kinetics by myosin light chain phosphorylation in rabbit skeletal muscle: implications for regulation of actin-myosin interaction. Proceedings of the National Academy of Sciences 1990;87(1):414–8.

Wahr PA, Metzger JM. Role of Ca^{2+} and cross-bridges in skeletal muscle thin filament activation probed with Ca^{2+} sensitizers. Biophysical journal 1999;76(4):2166–76.

Westerblad H, Allen D. Changes of myoplasmic calcium concentration during fatigue in single mouse muscle fibers. The Journal of General Physiology 1991;98(3):615–35.

Westerblad H, Allen DG. The contribution of [ca2+] i to the slowing of relaxation in fatigued single fibres from mouse skeletal muscle. The Journal of Physiology 1993;468(1):729–40.

Wu JZ, Herzog W, Cole GK. Modeling dynamic contraction of muscle using the cross-bridge theory. Math Biosci 1997;139(1):69–78.

Zahalak GI. A distribution-moment approximation for kinetictheories of muscular contraction. Mathematical Biosciences 1981;55:89–114.